Dalton Transactions

Cite this: *Dalton Trans.*, 2011, **40**, 6028

www.rsc.org/dalton

PAPER

A novel precursor system and its application to produce tin doped indium oxide

M. Veith,*[a,b] C. Bubel[a] and M. Zimmer[b]

Received 13th January 2011, Accepted 31st March 2011
DOI: 10.1039/c1dt10067j

A new type of precursor has been developed by molecular design and synthesised to produce tin doped indium oxide (ITO). The precursor consists of a newly developed bimetallic indium tin alkoxide, $Me_2In(O^tBu)_3Sn$ (Me = CH_3, O^tBu = $OC(CH_3)_3$), which is in equilibrium with an excess of $Me_2In(O^tBu)$. This quasi single-source precursor is applied in a sol–gel process to produce powders and coatings of ITO using a one-step heat treatment process under an inert atmosphere. The main advantage of this system is the simple heat treatment that leads to the disproportionation of the bivalent Sn(II) precursor into Sn(IV) and metallic tin, resulting in an overall reduced state of the metal in the final tin doped indium oxide (ITO) material, hence avoiding the usually necessary reduction step. Solid state ^{119}Sn-NMR measurements of powder samples confirm the appearance of Sn(II) in an amorphous gel state and of metallic tin after annealing under nitrogen. The corresponding preparation of ITO coatings by spin coating on glass leads to transparent conductive layers with a high transmittance of visible light and a low electrical resistivity without the necessity of a reduction step.

Introduction

Thin films of transparent conducting oxides (TCOs), especially tin doped indium oxide (ITO), are of high interest for a variety of applications as transparent electrodes, including display devices,[1,2] and electroluminescent and electrochromic applications such as LEDs, OLEDs,[3] electrochromic windows[4] and solar cells.[5] Additionally, ITO is also used in optical devices such as antireflective and antistatic coatings (ARAS), and gradient lenses, taking advantage of their high refractive index and high transmissivity.[6]

Compared to other TCO materials such as doped ZnO and SnO_2, ITO exhibits the best properties in terms of high electrical conductivity, appropriate optical transmission in the visible range of light, and good chemical and mechanical stability.[7] It is therefore the most widely used TCO material.

Thin films of ITO can be applied by sputtering techniques,[8,9] CVD processes,[10,11,12] spray pyrolysis[13,14] and the sol–gel process.[5,15,16,17] The processes usually require cost-effective and substrate size-restricting vacuum equipment for low oxygen partial-pressure deposition (sputtering, CVD) or post-treatment of the as-deposited and crystallised ITO layers (spray pyrolysis, sol–gel process) under reducing atmospheric conditions (*e.g.*, H_2, CO) to achieve the required high electrical conductivity. The conduction mechanism of ITO relies on the formation of a reduced metallic state inside the oxide lattice, which is usually interpreted as the creation of an oxygen deficiency situation.[18] This chemical treatment often results in drastic morphological changes of the oxide material, such as "overreduction" of the metals indium and tin due to surface-concentrated reduction of the layer and the creation of metallic areas, lowering the electrical and optical performance of the material.[19]

The aim of this work was to avoid this reduction step during the production of ITO (powders, coatings) in the sol–gel process. This process was chosen due to its capability of coating large and complex-shaped substrates in a low-cost and straightforward way. Additionally, the homogeneity of the dopand distribution (tin) in ITO is aimed to be improved by the use of bimetallic In-Sn alkoxides as single-source precursor materials.[20]

By combinations of elements at a molecular level, single-source precursors can prevent the segregation tendencies usually observed in multi-source precursors, which are due to different solubilities and activities when using two or more precursors.[21,22] The aim is to enable the direct incorporation of tin inside the In_2O_3 host lattice of ITO by using a quasi single-source precursor system.

Results and discussion

Synthesis of precursor

Alkoxides of indium and tin were chosen as starting materials. After refluxing a solution of $Me_2In(O^tBu)$ and $[Sn(O^tBu)_2]_2$ in toluene, the formation of a product was observed that could be distilled at 70 °C, giving a colourless liquid. The reaction product was characterised by NMR spectroscopy and chemical analysis. Depending on the stoichiometric amount of $Me_2In(O^tBu)$ in the reaction, the excess of $Me_2In(O^tBu)$ is included in the distillate, which becomes a waxy solid below 25 °C (eqn (1)).

[a]*INM – Leibniz Institute for New Materials, Campus D2 2, 66123 Saarbrücken, Germany. E-mail: Michael.veith@inm-gmbh.de; Fax: +49 681 9300 223; Tel: +49 681 9300 272*
[b]*Saarland University, Inorganic and General Chemistry, Campus C4 1, 66123 Saarbrücken, Germany*

$$9Me_2In(O^tBu) + \tfrac{1}{2}[Sn(O^tBu)_2]_2 \rightarrow Me_2In(O^tBu)_3Sn + 8Me_2In(O^tBu) \quad (1)$$

According to the NMR data, a new bimetallic, heteroleptic indium-tin alkoxide had been formed in an equilibrium reaction between $Me_2In(O^tBu)$ and $Sn(O^tBu)_2$ with two bridging and one terminal *tert*-butoxy groups (Fig. 1).

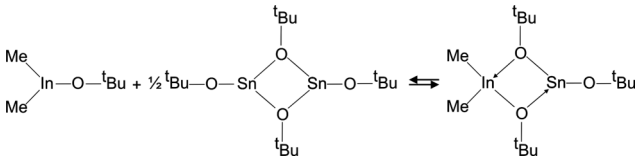

Fig. 1 Reaction scheme for the formation of $Me_2In(O^tBu)_3Sn$.

Temperature-dependent ^{13}C-NMR measurements in d_8-toluene show coalescence effects (Fig. 2). At low temperatures (< 230 K), the singlet signal of the methyl group of the product $Me_2In(O^tBu)_3Sn$ splits into two signals with an equal integration ratio. The two methyl groups at the indium centre are thus located in different electronic environments.

Additionally, the singlet of the primary carbon atoms of the *tert*-butoxy groups of $Me_2In(O^tBu)_3Sn$ splits into two signals with an integration ratio of 2 : 1, showing that the two bridging *tert*-butoxy groups are located in a different electronic environment to the single terminal *tert*-butoxy group at the tin atom.

At low temperatures, the organic ligands of $Me_2In(O^tBu)_3Sn$ are arranged in a well-defined way, which can be described as follows: the *tert*-butoxy group of $Me_2In(O^tBu)$ and one of the $Sn(O^tBu)_2$ form dative bonds towards the Lewis acidic (electrophilic) metal centres indium and tin. The two methyl groups attached to the tetrahedrally-coordinated indium atom are situated perpendicular to the bridging *tert*-butoxy groups and the metal centres that form a four-membered InO_2Sn ring are coplanar with the terminal *tert*-butoxy group at the tin atom (Fig. 3). Formulae A and B are two mesomeric borderline descriptions, the real state of the structure being an intermediate. Within the four-membered ring, one cannot distinguish between donor bonds and two-electron-two-centre bonds.

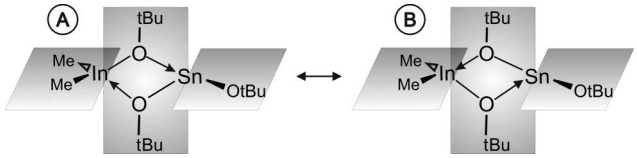

Fig. 3 Scheme of the arrangement (A and B) in $Me_2In(O^tBu)_3Sn$.

Upon raising the temperature, rearrangement of the ligands in the symmetrical molecule occur due to dynamic processes in solution (Fig. 4). This can be detected from the coalescence points observed in the spectra (see Fig. 2). Terminal and bridging *tert*-butoxy groups dynamically change positions by intramolecular rotations around bonds (processes 1 and 3 in Fig. 4). Additionally, the mesomeric structures of the product have to be considered (process 2).

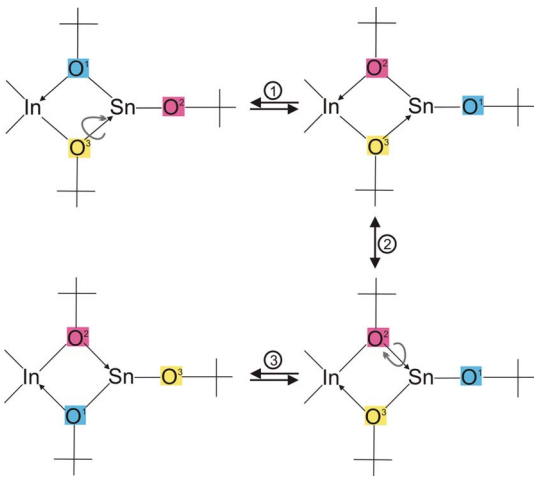

Fig. 4 Scheme of the rearrangement processes in $Me_2In(O^tBu)_3Sn$ in solution. Processes 1 and 3: intramolecular bonding rotations, process 2: contributing structures.

By varying the stoichiometry of $Me_2In(O^tBu)$ and $Sn(O^tBu)_2$, a new kind of precursor system can be designed in which its

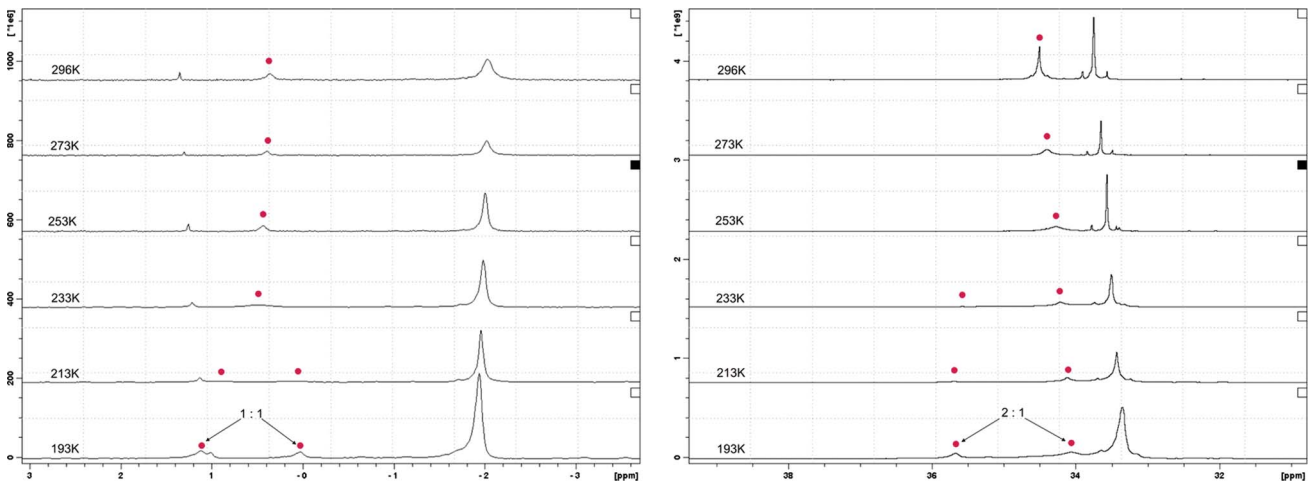

Fig. 2 ^{13}C-NMR spectra of the product at different temperatures (in K). Left: signal of the methyl group $In(CH_3)_2$ (red dots). Right: signal of the primary carbon of the *tert*-butoxy groups $C(CH_3)_3$ (red dots). Signals at –2 ppm (left) and at around 33 ppm (right) are related to the methyl group and the primary carbon of the *tert*-butoxy groups of $Me_2In(O^tBu)$. The small signal at ~1.4 ppm (left) results from by-products.

components are interconnected by a dynamic equilibrium between excess $Me_2In(O^tBu)$ and the newly developed, heteroleptic alkoxide $Me_2In(O^tBu)_3Sn$ (Fig. 5). The precursor is a colourless liquid above 30 °C and can be obtained in high purity and high yield by distillation, the mixture showing an azeotropic boiling point.

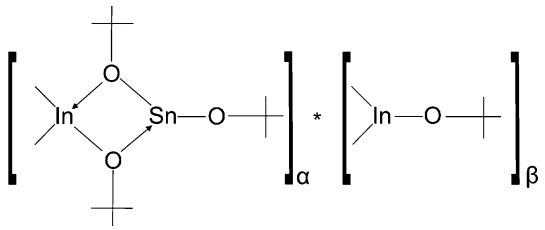

Fig. 5 Scheme of the ITO quasi single-source precursor $[Me_2In(O^tBu)_3Sn]_\alpha \cdot [Me_2In(O^tBu)]_\beta$.

This precursor system was used to produce powders and coatings of ITO, as described below.

Preparation of indium tin oxide powder

An alcoholic solution of the precursor with a final doping concentration of 10 atom% Sn was used in the sol–gel process by the addition of water. We also used 6 and 8 atom% Sn in other experiments, but will publish this data in a following paper.[23] After evaporation of all the volatile solvents at 110 °C in air, a colourless, amorphous powder could be obtained that changed colour to grey-blue after crystallisation under an inert atmosphere at 500 °C. Before and after tempering, samples of the powder were collected for solid-state ^{119}Sn-NMR measurements. The as-prepared material showed a broad peak centred around $\delta = -540$. The width of the peak indicated the amorphous state of the solid; the coordinated hydroxyl groups and water shift the signal of the tin(II) towards lower values, most likely forming a Sn(II)-oxy-hydroxide (Fig. 6).

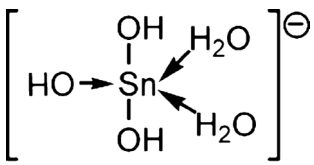

Fig. 6 Scheme of the coordinated Sn(II)-oxy-hydroxide.

After annealing under an inert atmosphere at 500 °C, the solid gel turned into a grey-blue powder. Solid-state ^{119}Sn-NMR was occluded by the appearance of a paramagnetic behaviour of the crystallised oxide owing to the formation of metallic tin Sn(0) together with Sn(IV) due to a disproportionation reaction of the bivalent tin in the precursor system during inert gas tempering. Elemental analysis of the blue powder showed only a slight contamination of the ITO powder with carbon (0.18%) and hydrogen (0.36%), and no inclusion of nitrogen (0%), which was used as an inert gas.

XRD measurements of the powder were consistent with the formation of cubic In_2O_3 with an average crystallite size of 20 nm, according to Scherrer's equation[24] (Fig. 7). No further crystalline phases could be observed. Cubic axis a in the doped In_2O_3 of 10.148(3) Å increased compared to the non-doped material (10.118(1) Å),[25] which had been expected.[26]

The crystallised ITO particles can be further used in redispersable coating solutions in wet chemical coating techniques.[27,28]

Preparation of indium tin oxide coatings

Sol–gel coatings of ITO on glass substrates could be prepared by spin-coating alcoholic solutions of the as-described precursor system with different concentrations of dopand tin. After deposition of the gel layers and annealing for 4 h under an inert atmosphere, ITO coatings of approximately 40 nm thickness could be obtained. A representative SEM image (one out of 10 different) of the film is shown in Fig. 8. XRD measurements (Fig. 9) and X-ray reflectometry analysis revealed a pure ITO phase of the layer (10 atom% Sn) with a crystallite size of 24 nm, according to Scherrer's equation, and a high coating density of 76.3%. No further phases such as SnO_2 could be detected. The ITO coatings produced show minimal haze (0.06%) and high thermal stability.

To compare the effect of this one-step annealing technique under an inert atmosphere with the conventional two-step process, including the reduction treatment, equally prepared gel layers were annealed under nitrogen (4 h, 500 °C) and in air (4 h, 500 °C), followed by reduction treatment (0.5 h, 300 °C, $N_2 : H_2$ 95 : 5), respectively. Ellipsometry measurements showed that the final thickness of the nitrogen annealed coatings (41 nm) and of the two-step annealed coatings (42 nm) were comparable.

As can be seen in the UV-vis-NIR transmission graph in Fig. 10, ITO coatings annealed only under a nitrogen atmosphere showed higher transmission in the visible range and an increased slope

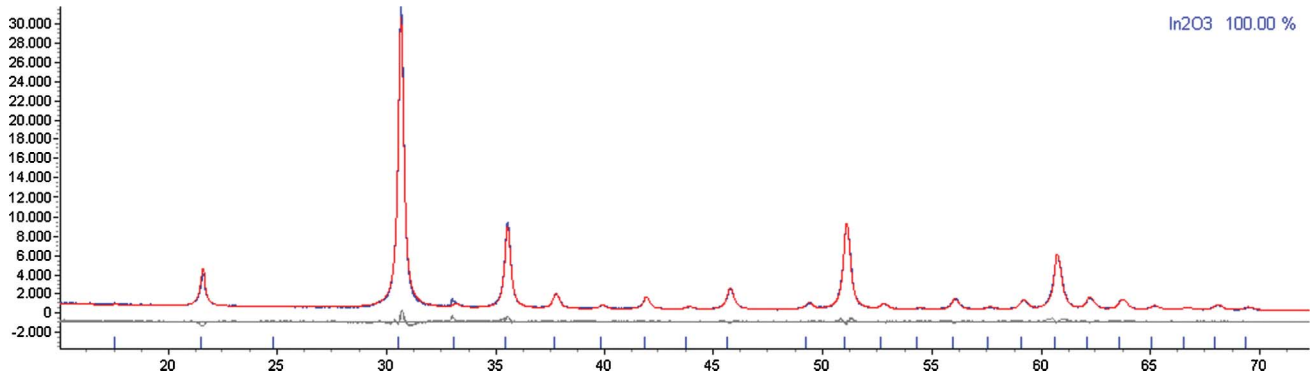

Fig. 7 Powder XRD pattern with Rietveld refinement (cubic In_2O_3) of the powder annealed under an inert atmosphere.

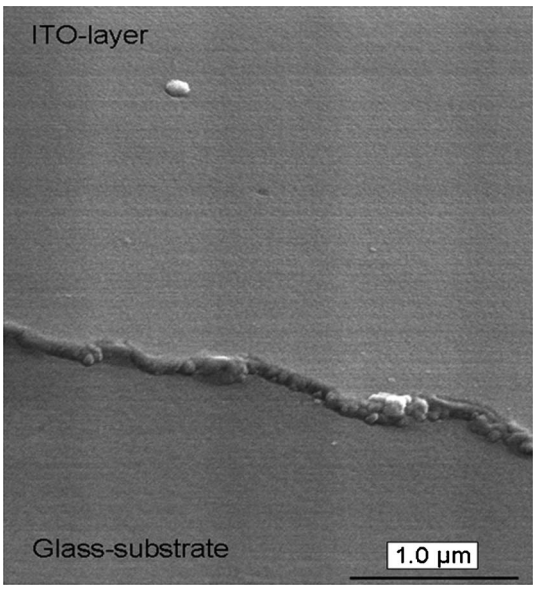

Fig. 8 SEM image of an ITO layer on a glass substrate (cut edge) after annealing under nitrogen.

of the plasma edge in the IR range. Based on the reflectivity measurements (not included), the reduced transmission can be attributed to an increased reflection of the nitrogen-annealed ITO coatings in the IR range compared to coatings post-treated under the forming gas.

The increased transmission of 91%, compared to 87% in the visible range, can be attributed to the lack of overreduced, metallic areas near the surface, which often appears when using the forming gas as a reducing agent, leading to a reduced transmission and cracks on the surface.

The improved reflectivity with infrared radiation is strongly correlated to an increased carrier density of the material.[29] In fact, resistivity measurements show that not only the optical performance in enhanced. The measured specific resistivity of the samples annealed in air and under the forming gas is 1.3×10^{-3} Ω cm. Samples taking advantage of the disproportionation reaction during the one-step tempering under an inert atmosphere

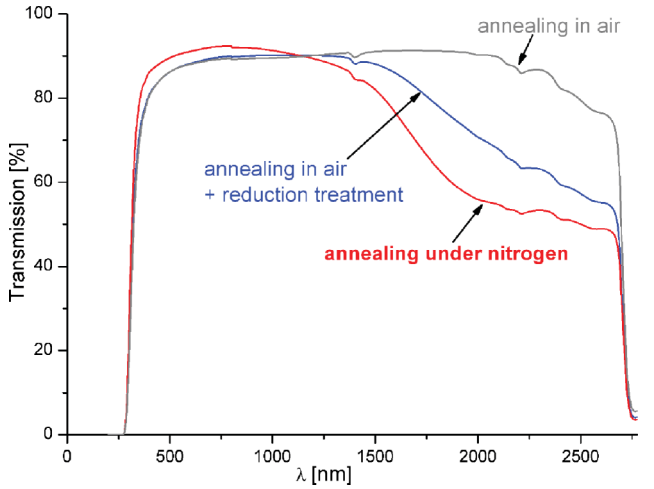

Fig. 10 A UV-vis-NIR diagram of ITO coatings after annealing in air (grey curve), after annealing in air with post-treatment under the forming gas (blue), and annealing under an inert atmosphere (red).

show a resistivity of only 1.1×10^{-3} Ω cm. This improvement can also be explained by the lack of metallic areas near the (reduced) surface, which leads to cracks and hence a lowering of the electrical conductivity of the ITO coating.

Conclusion

A novel type of precursor has been designed to produce ITO *via* a sol–gel process without using forming gas reduction. The system is based on a single-source precursor concept, consisting of the bimetallic In–Sn-alkoxide $Me_2In(O^tBu)_3Sn$, which is interconnected with an excess of reactant $Me_2In(O^tBu)$ to form an azeotrope and achieve the desired metal ratio of between 6–10 atom% Sn. The dynamic structure of the precursor system has been analysed by NMR spectroscopy. Applying the precursor in the sol–gel process and tempering the gel under an inert atmosphere leads to the disproportionation of the bivalent tin in the precursor, thus establishing a reduced state inside the ITO. This effect makes post-treatment of the crystallised material under

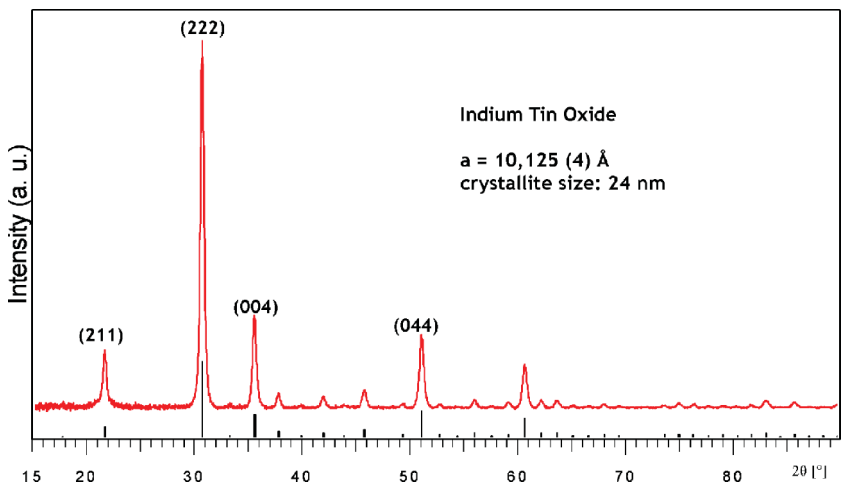

Fig. 9 XRD pattern with Rietveld refinement of the ITO coating (40 nm thickness) after annealing under an inert atmosphere; reference lines according to cubic In_2O_3; crystallite size calculated from Scherrer's equation.

reducing atmospheres redundant. Sol–gel coatings produced by this technique show excellent optical properties, as well as improved electrical conductivity.

Experimental

General

All chemical reactions were performed under nitrogen atmosphere using a Schlenk apparatus. Solvents (diethylether, toluene) were distilled from sodium and kept under nitrogen. $[Sn(O^tBu)_2]_2$ was prepared according to a literature procedure.[30] $Me_2In(O^tBu)$ was prepared from a salt elimination reaction between Me_2InCl and $Li(O^tBu)$ in an equimolar ratio in diethylether and purified by sublimation, leading to a colourless waxy solid.

Synthesis of $Me_2In(O^tBu)_3Sn$

To a solution of $Me_2In(O^tBu)$ (3.8 g, 17.43 mmol) in 25 ml toluene was added dropwise a solution of $[Sn(O^tBu)_2]_2$ (4.6 g, 8.72 mmol) in 25 ml toluene. After 12 h of refluxing, the solvent was removed under a reduced pressure. The remaining product could be distilled at 70 °C under vacuum leading to a colourless liquid. Waxy fractions were attributed to excess of $Me_2In(O^tBu)$ (see the discussion).

Analysis: $C_{14}H_{33}InO_3Sn$ (482.94): In 23.14 (calc. 23.78), Sn 24.09 (calc. 24.58)%.

^{1}H-NMR (C_6D_6) δ = 0.08 (s, 6H, In(CH_3)), 1.33 (s, 27H, C(CH_3)$_3$); ^{13}C-NMR (C_6D_6): δ = 0.4 (s, 2C, In(CH_3)), 33.57 (s, 9C, C(CH_3)$_3$), 71.73 (s, 3C, C(CH$_3$)$_3$); ^{119}Sn-NMR (C_6D_6): δ = −168,25 ppm (s, 1 Sn). For temperature dependent ^{13}C-NMR spectra, see Fig. 2.

Preparation of indium tin oxide

ITO powder. A precursor system with a doping concentration of 10 atom% Sn (according to the total amount of In and Sn) was obtained by mixing $Me_2In(O^tBu)_3Sn$ with an excess of $Me_2In(O^tBu)$ kept under a nitrogen atmosphere and dissolved in isopropanol to give a concentration of 0.4 mol l^{-1}. Under constant stirring, a mixture of water and isopropanol (1/2) was added dropwise to the precursor solution until the formation of a colourless precipitate was observed. After further stirring for 1 h under a nitrogen atmosphere, the suspension was kept stirring in air at 50 °C until all the liquid components had evaporated. The remaining colourless powder was further dried at 110 °C in air.

The as-prepared xerogel is then annealed in pure nitrogen gas (100 l h^{-1}) for 4 h at 500 °C (heating rate 100 °C h^{-1}). After annealing, the colour of the powder had turned to grey-blue. The XRD pattern of the powder (Fig. 7) showed cubic In_2O_3 with a = 10.148(3) Å.

ITO coatings. Coating solutions were prepared by dissolving the precursor system in a preset metal ratio of 10 atom% Sn in a 1 : 1 mixture of isopropanol and 1-butanol to give a 0.4 molar coating solution. Substrates of borosilicate glass (Borofloat, 60 × 60 mm) were polished with a slurry of CeO_2 powder and cleaned in a professional washing machine (Miele IR 6001).

Coatings were produced by the spin-coating technique using 800 µl of coating solution and a spinning speed of 1000 rpm for 20 s. The as-prepared samples were placed in a furnace at 500 °C for 4 h under a flux of purified nitrogen gas (100 l h^{-1}). XRD characterisation showed cubic In_2O_3 with a = 10.125(4) Å.

Methods. Variable temperature NMR spectra were recorded in d_8-toluene on a Bruker Avance 400 spectrometer. Room temperature NMR measurements were recorded on 5% solutions of C_6D_6 in toluene on Bruker AC 200 F (^{1}H, ^{13}C) and AC 200 P (^{119}Sn) instruments. Solid state NMR measurements were performed on a Bruker MSL 200 instrument. X-Ray diffraction patterns were collected on a Siemens D500 diffractometer with Cu-Kα radiation. The determination of crystalline phases was based on the JCPDS database. Estimations of crystallite size were calculated according to Scherrer's equation.[24] X-Ray reflectometry measurements were performed on an X'Pert MRD diffractometer (now PANalytical) and refined with a Bruker AXS D8 powder diffractometer using an angle range between 0 and 3° in 0.004° steps. The thickness of coatings was recorded on an M-2000/A-SE ellipsometer by J. A. Woollam Co. Inc. UV-vis-NIR spectra were recorded on a Varian Cary 5000 instrument in transmission mode. The determination of specific sheet resistivity was done with a four point probe multimeter 34401A from Hewlett-Packard, taking the average of at least five measurements for each sample after annealing. Elemental analysis of metals was performed with a Jobin Yvon Ultima 2 ICP-AES apparatus.

References

1 J. I. Pankove, *Display Devices Topics in Applied Physics*, Springer-Verlag, Berlin, vol. 40, 1980.
2 T. Omata, M. Kita and H. Ikawa, *Thin Solid Films*, 2006, **503**, 22.
3 A. Cipran and F. E. Karasz, *J. Appl. Polym. Sci.*, 2006, **99**, 3125.
4 J. H. Burroughes, D. D. C. Bradley, A. R. Brown, R. N. Marks, K. Mackay, R. H. Friend, P. L. Burns and A. B. Holmes, *Nature*, 1990, **347**, 539.
5 M. J. Alam and D. C. Cameron, *Thin Solid Films*, 2002, **420–421**, 76.
6 A. Solieman and M. A. Aegerter, *Thin Solid Films*, 2006, **502**, 205.
7 M. J. Alam and D. C. Cameron, *Thin Solid Films*, 2000, **377–378**, 455.
8 Y. Shigesato and D. C. Paine, *Thin Solid Films*, 1994, **238**, 44.
9 T. Suzuki, *J. Mater. Sci. Lett.*, 1988, **7**, 79.
10 M. J. Hampden-Smith and T. T. Kodas, *Chem. Vap. Deposition*, 1995, **1**, 8.
11 K. L. Choy, *Prog. Mater. Sci.*, 2003, **48**, 57.
12 T. Muruyama and K. Fukui, *Thin Solid Films*, 1991, **203**, 297.
13 C. H. Lee and C. S. Huang, *Mater. Sci. Eng.*, 1994, **B22**, 223.
14 M. Rami, E. Benamar, C. Messaoudi, D. Sayah and A. Ennaoui, *Eur. J. Solid State Inorg. Chem.*, 1998, **35**, 211.
15 K. L. Chopra, S. Major and D. K. Pandya, *Thin Solid Films*, 1983, **102**, 1.
16 R. B. Hadj Tahar, T. Ban, Y. Ohya and Y. Takahashi, *J. Appl. Phys.*, 1998, **83**, 2631.
17 S. R. Ramanan, *Thin Solid Films*, 2001, **389**, 207.
18 G. Frank and H. Köstlin, *Appl. Phys. A: Solids Surf.*, 1982, **27**, 197.
19 G. Guenther, G. Schierming, R. Theissmann, R. Kruk, R. Schmechel, C. Baehtz and A. Prodi-Schwab, *J. Appl. Phys.*, 2008, **104**, 034501.
20 M. Veith, *J. Chem. Soc., Dalton Trans.*, 2002, 2405.
21 J. G. Na, Y. R. Cho, Y. H. Kim and T. D. Lee, *J. Am. Ceram. Soc.*, 1989, **72**, 698.
22 H. Morikawa, H. Kurata and M. Fujita, *J. Electron Microsc.*, 2000, **49**, 67.
23 M. Veith, C. Bubel and I. Grobelsek, to be published.
24 A. L. Patterson, *Phys. Rev.*, 1939, **56**, 978.
25 M. Marezio, *Acta Crystallogr.*, 1966, **20**, 723.
26 Y. Shigesato, Y. Hayashi and T. Haranoh, *Appl. Phys. Lett.*, 1992, **61**, 73.
27 C. Goebbert, R. Nonninger, M. A. Aegerter and H. Schmidt, *Thin Solid Films*, 1999, **351**, 79.
28 N. Al-Dahoudi and M. A. Aegerter, *Thin Solid Films*, 2006, **502**, 193.
29 C. G. Granqvist, *Appl. Phys. A: Solids Surf.*, 1993, **57**, 19.
30 M. Veith and F. Töllner, *J. Organomet. Chem.*, 1983, **246**, 219.

